

AFRL-ML-WP-TP-2006-409

**IMPROVEMENT OF DELAMINATION
RESISTANCE IN COMPOSITE
LAMINATES WITH NANO-
INTERLAYERS (PREPRINT)**



Sangwook Sihm, Jin W. Park, Ran Y. Kim, and Ajit K. Roy

JANUARY 2006

Approved for public release; distribution is unlimited.

STINFO COPY

This work, resulting in whole or in part from Department of the Air Force contract number FA8650-05-D-5052, has been submitted to the *Journal of Composite Materials* (Sage Publications). If this work is published, Sage Publications may assert copyright. The United States has for itself and others acting on its behalf an unlimited, paid-up, nonexclusive, irrevocable worldwide license to use, modify, reproduce, release, perform, display, or disclose the work by or on behalf of the Government. All other rights are reserved by the copyright owner.

**MATERIALS AND MANUFACTURING DIRECTORATE
AIR FORCE RESEARCH LABORATORY
AIR FORCE MATERIEL COMMAND
WRIGHT-PATTERSON AIR FORCE BASE, OH 45433-7750**

NOTICE AND SIGNATURE PAGE

Using Government drawings, specifications, or other data included in this document for any purpose other than Government procurement does not in any way obligate the U.S. Government. The fact that the Government formulated or supplied the drawings, specifications, or other data does not license the holder or any other person or corporation; or convey any rights or permission to manufacture, use, or sell any patented invention that may relate to them.

This report was cleared for public release by the Air Force Research Laboratory Wright Site (AFRL/WS) Public Affairs Office and is available to the general public, including foreign nationals. Copies may be obtained from the Defense Technical Information Center (DTIC) (<http://www.dtic.mil>).

AFRL-ML-WP-TP-2006-409 HAS BEEN REVIEWED AND IS APPROVED FOR PUBLICATION IN ACCORDANCE WITH ASSIGNED DISTRIBUTION STATEMENT.

//Signature//

AJIT K. ROY, Program Manager
Structural Materials Branch
Nonmetallic Materials Division

//Signature//

TIA BENSON TOLLE, Chief
Structural Materials Branch
Nonmetallic Materials Division

//Signature//

PERSIS A. ELWOOD, Deputy Chief
Nonmetallic Materials Division
Materials and Manufacturing Directorate

This report is published in the interest of scientific and technical information exchange, and its publication does not constitute the Government's approval or disapproval of its ideas or findings.

REPORT DOCUMENTATION PAGE				<i>Form Approved</i> OMB No. 0704-0188	
<p>The public reporting burden for this collection of information is estimated to average 1 hour per response, including the time for reviewing instructions, searching existing data sources, gathering and maintaining the data needed, and completing and reviewing the collection of information. Send comments regarding this burden estimate or any other aspect of this collection of information, including suggestions for reducing this burden, to Department of Defense, Washington Headquarters Services, Directorate for Information Operations and Reports (0704-0188), 1215 Jefferson Davis Highway, Suite 1204, Arlington, VA 22202-4302. Respondents should be aware that notwithstanding any other provision of law, no person shall be subject to any penalty for failing to comply with a collection of information if it does not display a currently valid OMB control number. PLEASE DO NOT RETURN YOUR FORM TO THE ABOVE ADDRESS.</p>					
1. REPORT DATE (DD-MM-YY) January 2006		2. REPORT TYPE Journal Article Preprint		3. DATES COVERED (From - To)	
4. TITLE AND SUBTITLE IMPROVEMENT OF DELAMINATION RESISTANCE IN COMPOSITE LAMINATES WITH NANO-INTERLAYERS (PREPRINT)				5a. CONTRACT NUMBER FA8650-05-D-5052	
				5b. GRANT NUMBER	
				5c. PROGRAM ELEMENT NUMBER 62102F	
6. AUTHOR(S) Sangwook Sihn, Jin W. Park, and Ran Y. Kim (University of Dayton Research Institute) Ajit K. Roy (AFRL/MLBC)				5d. PROJECT NUMBER 4347	
				5e. TASK NUMBER RG	
				5f. WORK UNIT NUMBER M03R1000	
7. PERFORMING ORGANIZATION NAME(S) AND ADDRESS(ES) University of Dayton Research Institute 300 College Park Dayton, OH 45469-0168				8. PERFORMING ORGANIZATION REPORT NUMBER	
Structural Materials Branch (AFRL/MLBC) Nonmetallic Materials Division Materials and Manufacturing Directorate Air Force Research Laboratory, Air Force Materiel Command Wright-Patterson Air Force Base, OH 45433-7750					
9. SPONSORING/MONITORING AGENCY NAME(S) AND ADDRESS(ES) Materials and Manufacturing Directorate Air Force Research Laboratory Air Force Materiel Command Wright-Patterson AFB, OH 45433-7750				10. SPONSORING/MONITORING AGENCY ACRONYM(S) AFRL-ML-WP	
				11. SPONSORING/MONITORING AGENCY REPORT NUMBER(S) AFRL-ML-WP-TP-2006-409	
12. DISTRIBUTION/AVAILABILITY STATEMENT Approved for public release; distribution is unlimited.					
13. SUPPLEMENTARY NOTES Journal article preprint submitted to the Journal of Composite Materials (Sage Publications). This work resulted in whole or in part from Department of the Air Force contract number FA8650-05-D-5052. This paper contains color. PAO Case Number: AFRL/WS 06-0281, 2 Feb 06.					
14. ABSTRACT Interlaminar damage in the form of delamination due to the stress concentration is one of the dominant forms in laminated composite structures. One of the approaches to enhance the delamination resistance of the advanced composite structures is to reduce mismatch of elastic properties and the stress concentrations at the interfaces between the laminated layers by utilizing interleave materials. The interleave material considered in this study is a nano-interlayer which can be fabricated in the form of either a thin film of nano-modified epoxy reinforced with vapor grown nanofibers or a fiber mat that can be fabricated with the electrospun fiber process. The nanofibers in the form of a thin film are functionalized with ozone to enhance the interfacial strength between the nanofibers and the surrounding epoxy. To computationally assess the effectiveness of this approach, continuous interface elements of zero thickness are utilized for the characterization of the nano-interlayer. The interface element formulation is based on a cohesive zone model with softening constitutive law. Meanwhile, the experiment was performed with two types of nano-interlayers that are inserted into the laminated composites to monitor initiation and progression of their damage behavior.					
15. SUBJECT TERMS micro cracking, thermomechanical loadings, finite element analysis					
16. SECURITY CLASSIFICATION OF:			17. LIMITATION OF ABSTRACT: SAR	18. NUMBER OF PAGES 22	19a. NAME OF RESPONSIBLE PERSON (Monitor) Ajit K. Roy 19b. TELEPHONE NUMBER (Include Area Code) N/A
a. REPORT Unclassified	b. ABSTRACT Unclassified	c. THIS PAGE Unclassified			

IMPROVEMENT OF DELAMINATION RESISTANCE IN COMPOSITE LAMINATES WITH NANO-INTERLAYERS

Sangwook Sihh,¹ Jin W. Park,¹ Ran Y. Kim¹ and Ajit K. Roy²

¹University of Dayton Research Institute
300 College Park, Dayton, OH 45469-0168, USA

²Air Force Research Laboratory, AFRL/MLBC
Wright-Patterson AFB, OH 45433-7750, USA

ABSTRACT

Interlaminar damage in the form of delamination due to the stress concentration is one of the dominant forms of damage in laminated composite structures. One of the approaches to enhance the delamination resistance of the advanced composite structures is to reduce mismatch of elastic properties and stress concentrations at the interfaces between the laminated layers by utilizing interleave materials. The interleave material considered in this study is a nano-modified epoxy reinforced with vapor-grown nanofibers. The nanofibers are functionalized with ozone to enhance the interfacial strength between the nanofibers and the surrounding epoxy.

To numerically assess the effectiveness of this approach, continuous interface elements of zero thickness are utilized for the characterization of the nano-modified layer. The interface element formulation is based on a cohesive zone model with softening constitutive law. The numerical study is carried out with a focus on the composite laminates with a stacking sequence of $[30/-30/90/90/-30/30]_T$ under uniaxial tensile loading. The stress analysis shows that the laminates with such a layup can have large interlaminar stress components. Three-dimensional finite element analyses are carried out with the interface elements being placed along the ply interfaces, and the results are compared with the available experimental data.

Computational and experimental studies were carried out for the laminated composites reinforced with nano-interlayers that were fabricated in the form of either a thin film of nano-modified epoxy reinforced with vapor-grown nanofibers or a fiber mat that can be fabricated with the electrospun fiber process. The computation model used a cohesive zone model with interface elements based on bilinear and exponential constitutive laws. The model was used to simulate mode I, mode II and mixed-mode fracture tests to assess initiation and progression of delamination characteristics of the laminated composites.

From a numerical parametric study for the mode I fracture with a double cantilever beam (DCB) test, we found that the maximum load is mostly dependent on the critical energy release rate

(G_{IC}) with the bilinear constitutive law. Interfacial strength and penalty parameter play fewer roles in determining the maximum load. Parametric studies were carried out for mode II, an end notch flexure (ENF) test, to assess the delamination characteristics corresponding to different parameters of the exponential constitutive law. Finally, uniaxial tension simulations were carried out for the [-30/30/90/NL]_s specimen to predict the free-edge delamination characteristics corresponding to different interface properties.

Experimental observation from micrographs and stress-strain behavior shows that the laminated composites with the nano-interlayers can suppress the stress concentration and severity of the microcrack and delamination damage.

KEY WORDS: Microcracking, Thermomechanical Loadings, Finite Element Analysis.

1 INTRODUCTION

Interlaminar damage in the form of delamination due to the stress concentration is one of the dominant forms of damage in laminated composite structures. One of the approaches to enhance the delamination resistance of the advanced composite structures is to reduce mismatch of elastic properties and the stress concentrations at the interfaces between the laminated layers by utilizing interleave materials. The interleave material considered in this study is a nano-interlayer which can be fabricated in the form of either a thin film of nano-modified epoxy reinforced with vapor-grown carbon nanofibers (VGCNFs) or a fiber mat that can be fabricated with the electrospun fiber process. The nanofibers in the form of a thin film are functionalized with ozone to enhance the interfacial strength between the nanofibers and the surrounding epoxy.

To computationally assess the effectiveness of this approach, continuous interface elements of zero thickness are utilized for the characterization of the nano-interlayer. The interface element formulation is based on a cohesive zone model with softening constitutive law. Meanwhile, the experiment was performed with two types of nano-interlayers that are inserted into the laminated composites to monitor initiation and progression of their damage behavior. The first section illustrates the formulation of the computational cohesive zone model and the results of the parametric study. The next section illustrates the experimental observation.

2 COMPUTATION

A cohesive zone model (CZM) has gained much attention in predicting the delamination in laminated composites structures. The CZM uses an interface element based on a softening constitutive law. The advantage of the CZM approach originates from the constitutive model of the interface zone that directly relates the opening displacement jump to the traction force and thus avoids stress singularity problems. The CZM for predicting the initiation and progression of the delamination in laminated composites was developed with an interface element that is implemented in a finite element (FE) program. The model uses bilinear and exponential softening constitutive laws that describe the load vs. crack opening displacement behaviors. Parallel implementation for solving nonlinear finite element equations with interface elements

was tested and validated. The parallelization of the finite element program is beneficial both in terms of computational efficiency and ability to handle large problems. Also, we implemented and tested the exponential constitutive law which can be more reliable to obtain the converged solution than the bilinear constitutive law. This section illustrates the derivation of the computational model and the numerical results as well as the parametric study with various input parameters.

2.1 Constitutive relations of the interfacial zone

The CZM incorporates the softening constitutive behavior that relates the displacement jump to the traction force in the interface. The shape of the softening constitutive relation of CZM is derived from empirical observations and allows it to represent material degradation near a crack tip without having to directly deal with the singular stress fields of linear fracture mechanics. Among several constitutive models adopted in developing the interface elements to simulate delamination, bilinear (developed by Camanho, et al. [1]) and exponential (developed by Goyal, et al. [2]) constitutive models are adopted in the present study. Both models are capable of handling mixed-mode delamination and account for the irreversibility of the damage process. Equations for the two constitutive models are given in the remainder of this section.

To achieve accurate prediction of onset and growth of the delamination, especially for complex three-dimensional composite structures, sufficiently refined FE meshes are required especially in the direction of delamination propagation. Furthermore, the class of nonlinear problems involving softening constitutive law often exhibit sharp nonlinearities and requires many iterations with the nonlinear solution methods such as a Newton-Raphson method to obtain convergence at each load step. Therefore, a high-performance computing technology is harnessed to carry out the computer-intensive nonlinear analysis efficiently. The interface elements are implemented in a parallel FE program. It is characterized by incorporation of a memory- and computing-efficient multifrontal solver [3] in an object-oriented interpreter layer in a Python computer programming language and parallel computation of residual force vectors during iterations.

2.2 Numerical results and parametric study

Mode I fracture

We predicted a mode I fracture behavior with the CZM model. The model simulated a double cantilever beam (DCB) test configuration as shown in Figure 1. The stacking sequence of the lamination is $[+30/-30/90/NL/90/-30/+30]_T$ where NL is a nano-interlayer with prescribed partially delaminated zone between the $[90/90]$ interface surface. The stress analysis shows that the laminates with such a layup can have large interlaminar stress components that contribute to the delamination damage. The composite layer is made with a carbon-fiber reinforced epoxy material whose properties are listed in Table 1.

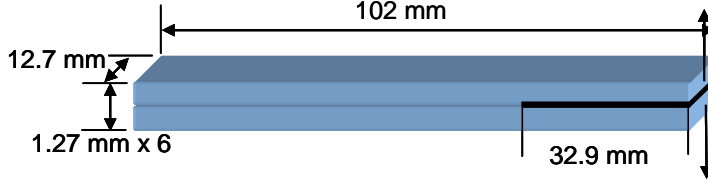


Figure 1.
Configuration of a
double-cantilever
beam test.

Table 1. Material properties of a carbon-fiber reinforced epoxy material

E_{11}	$E_{22} = E_{33}$	$G_{12} = G_{13}$	G_{23}	$\nu_{12} = \nu_{13}$
179.95 GPa	9.856 GPa	6.0674 GPa	3.3998 GPa	0.37
ν_{23}	G_{IC}	G_{IIC}	τ_3^o	$\tau_1^o = \tau_2^o$
0.45	-	-		

The first case considered is the bilinear softening constitutive law. Several parameters determine the shape of the bilinear law, and these are interlaminar strength (τ_3^o), penalty parameter (K), critical strain energy release rate (G_{IC}), critical stretching length (Δ_c) and final stretching length (Δ_p). τ_3^o and Δ_c are the load and displacement at the peak point of the bilinear curve, respectively. K is a slope of the increasing portion of the line. G_{IC} is the area under the bilinear curve. τ_3^o and Δ_c are related with the initiation of the delamination, and G_{IC} is related with progression of the delamination. Note that a ratio Δ_c/Δ_p indicates brittleness of the material. Among these parameters, not all of them are independent. For example, the penalty parameter is related with the interlaminar strength and the critical stretching length by $K = \tau_3^o/\Delta_c$, and the strain energy release rate is expressed with $G_{IC} = \tau_3^o\Delta_p/2$.

Three different bilinear softening constitutive laws were used for the simulation for a parametric study. The three cases are

- I. same K and Δ_p , different τ_3^o , Δ_c and G_{IC} (see Figure 2 (a)),
- II. same K and G_{IC} , different τ_3^o , Δ_c and Δ_p (see Figure 2 (b))
- III. same Δ_c and Δ_p , different K , τ_3^o and G_{IC} (see Figure 2 (c)).

Figure 2 shows the bilinear laws of three cases. On the right side of the figures are tables that list three different values of the parameters. Note that cases I and II use $K = 10^6$ N/mm³.

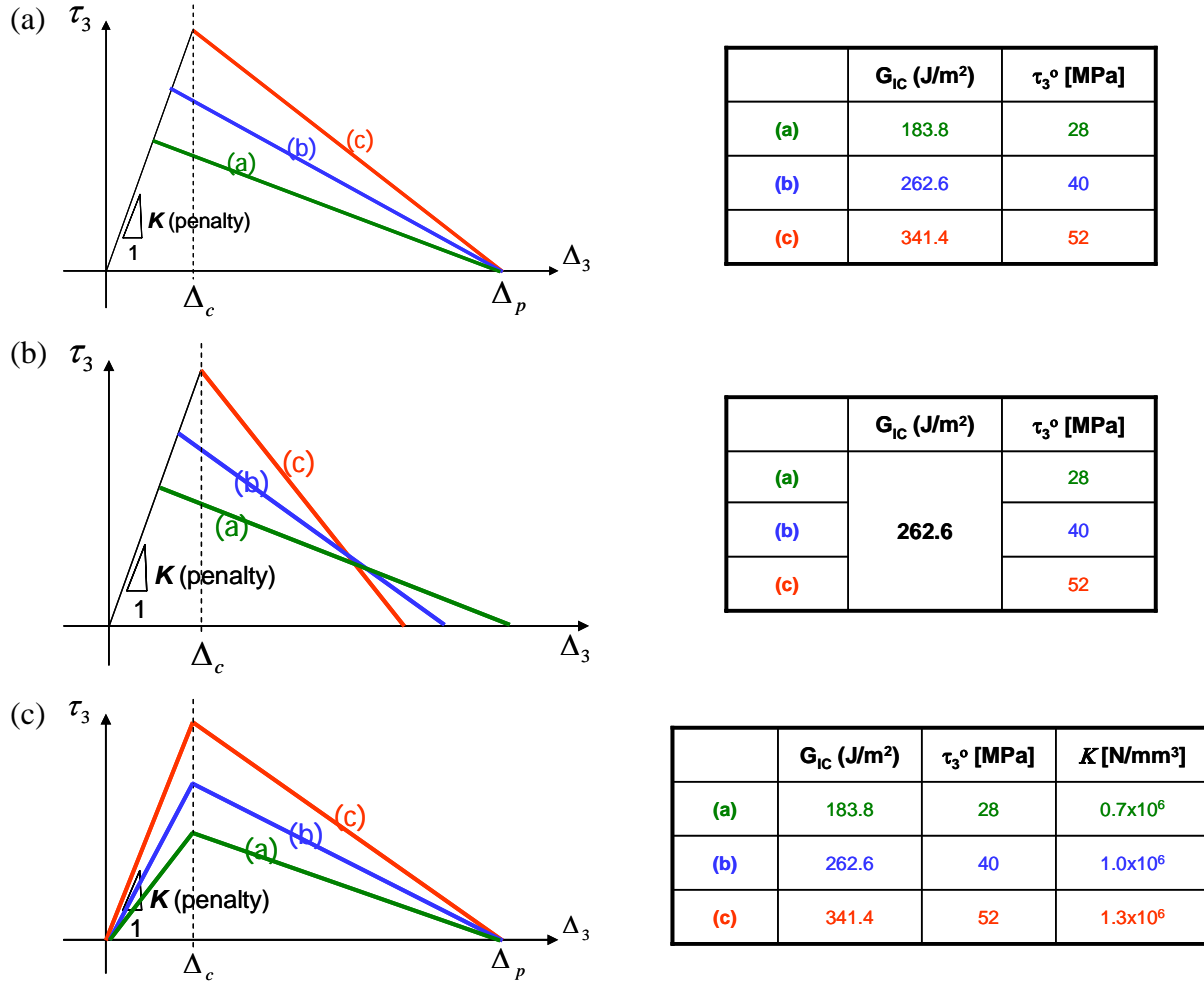


Figure 2. Three different bilinear softening constitutive laws with three different cases. (a) Case I with same K and Δ_p , different τ_3° , Δ_c and G_{IC} , (b) case II with same K and G_{IC} , different τ_3° , Δ_c and Δ_p and (c) case III with same Δ_c and Δ_p , different K , τ_3° and G_{IC} .

Figure 3 shows load-displacement curves under the DCB tests by using the three different bilinear constitutive laws in Figure 2. The maximum peak loads (P) in the figures are dependent on the parameters varied in the parametric study. From Figure 3 (a) and (b), higher τ_3° and G_{IC} results in higher maximum loads. It is interesting to note that case (2), which is under the condition of the same K and G_{IC} but different τ_3° , Δ_c and Δ_p , results in nearly identical maximum loads. Therefore, we can conclude that the maximum load is not sensitive to τ_3° , Δ_c and Δ_p but highly dependent on K and/or G_{IC} . The independence of the maximum load on τ_3° and Δ_c indicates that the global behavior of the DCB specimen under the mode I fracture loading is not sensitive to the initiation of the delamination damage.

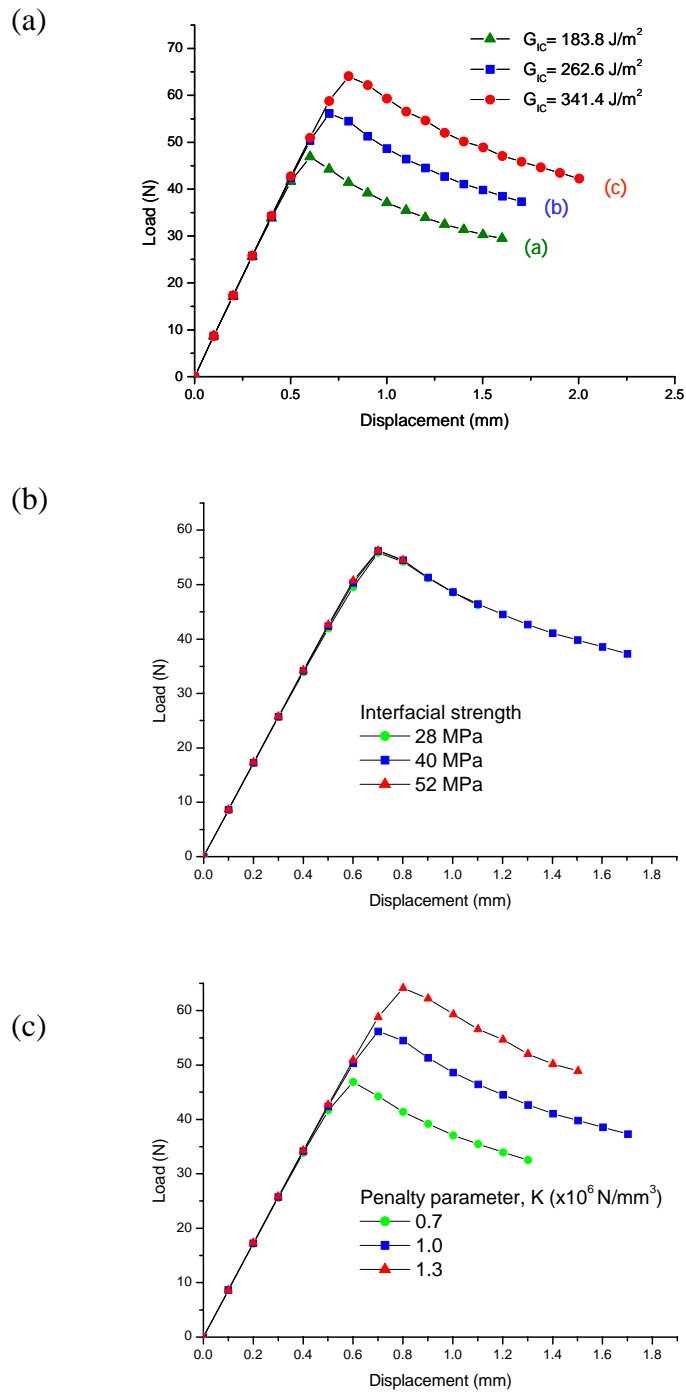


Figure 3. Prediction of mode I fracture under a DCB test with three different cases. (a) Case I in Figure 2 (a), (b) case II in Figure 2 (b) and (c) case III in Figure 2 (c).

Figure 4 shows a comparison of the results from case I and case III, which describes the bilinear constitutive laws with the same initial slope (K) and the same starting stretching displacement (Δ_c), respectively. Both the maximum load vs. G_{IC} in Figure 4 (a) and the maximum load vs. τ_3^o in Figure 4 (b) curves of cases I and III are identical. Therefore, we can conclude that the maximum load is not sensitive to K , Δ_c or the shape of the bilinear curves. From this conclusion and the one observed earlier, we can conclude that the maximum load is mostly dependent on the critical strain energy release rate (G_{IC}). The interfacial strength and penalty parameter play fewer roles in determining the maximum load. This is an important observation because we only need to pay attention to obtain the accurate G_{IC} from the experiment, especially when measuring the interfacial strength is a tough task.

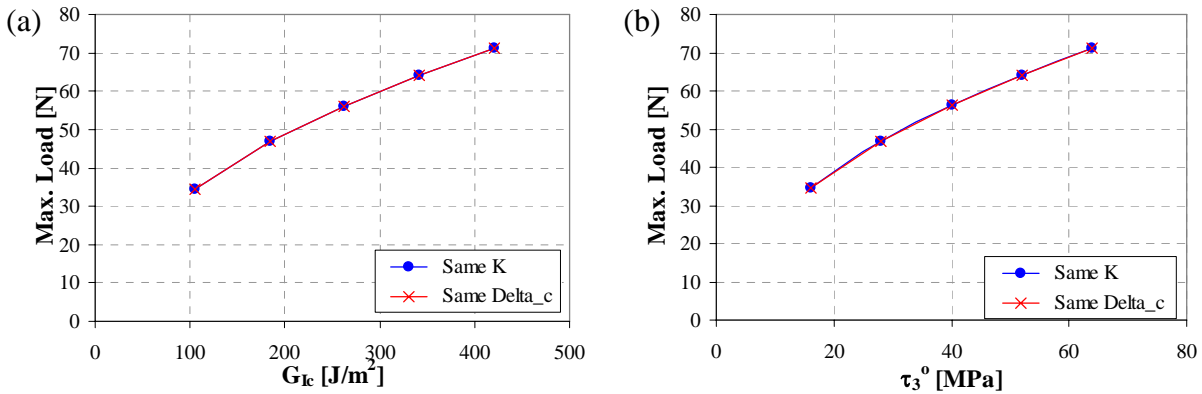


Figure 4. Comparison of case I and case III in Figure 2. (a) max. load vs. G_{IC} and (b) max. load vs. τ_3^o . Same K and same Δ_c indicate case I and III, respectively.

Mode II fracture

For mode II delamination, we simulated an ENF model using the exponential cohesive constitutive law (see Figure 5). An isotropic material property with $E = 150$ GPa and $\nu = 0.25$ was used for the numerical analyses. The ENF specimen was discretized using 100 elements in the axial direction, and the interface elements with exponential CZM were placed in the interlayer.

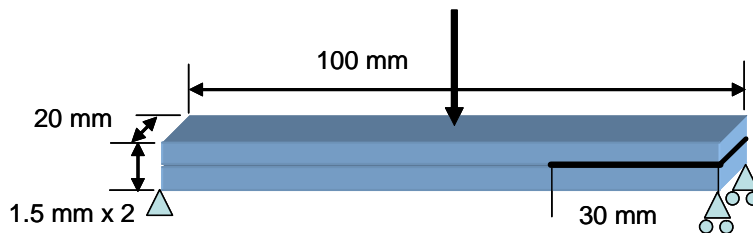


Figure 5. Configuration of an ENF test.

Several parameters determine the shape of exponential constitutive law. In case of mode II failure, these include an interfacial strength (τ_1^0) which defines the peak value of the traction-displacement curve, a critical energy release rate (G_{IIc}) which is the area under the curve, and a shape parameter (β) which determines the general shape of the exponential curve. Figure 6 shows the traction-displacement curves with three different shape parameters. Parametric studies were conducted to see the effect of these parameters on the mode II response of the ENF test specimen.

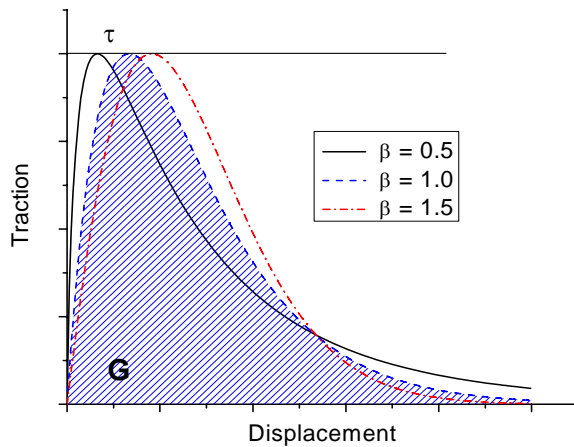


Figure 6.
Traction-displacement curves of exponential constitutive model with three different shape parameters (β).

Figure 7 shows the load-displacement response and the initial peak load of the ENF specimens for different values ranging of G_{IIc} from 0.68 N/mm to 2.32 N/mm. Correlation between initial peak load and G_{IIc} can be observed for the Mode II failure with the exponential model.

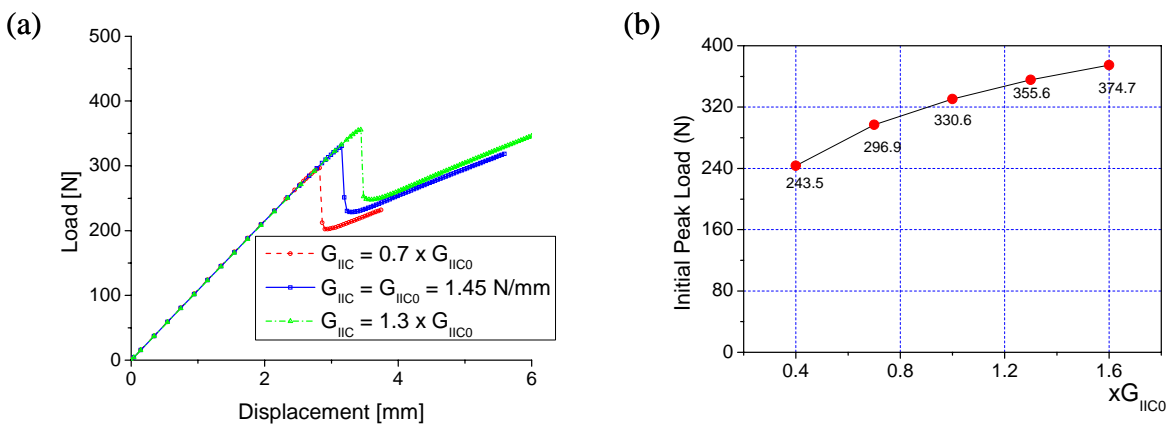


Figure 7. Response of the ENF specimens; (a) load displacement curve, and (b) initial peak load for different G_{IC} values.

Plots in Figure 8 depict the effect of different interfacial strength and β on the initial peak load value. The critical energy release rate is kept constant ($G_{IC} = 1.25 \text{ N/mm}$) for the parametric studies. While the previous results of Mode I with the bilinear constitutive model showed peak load was determined by G_{IC} , different peak values could be observed by varying the parameters that determine the shape of the exponential constitutive model although a constant G_{IC} was used for the ENF simulation.

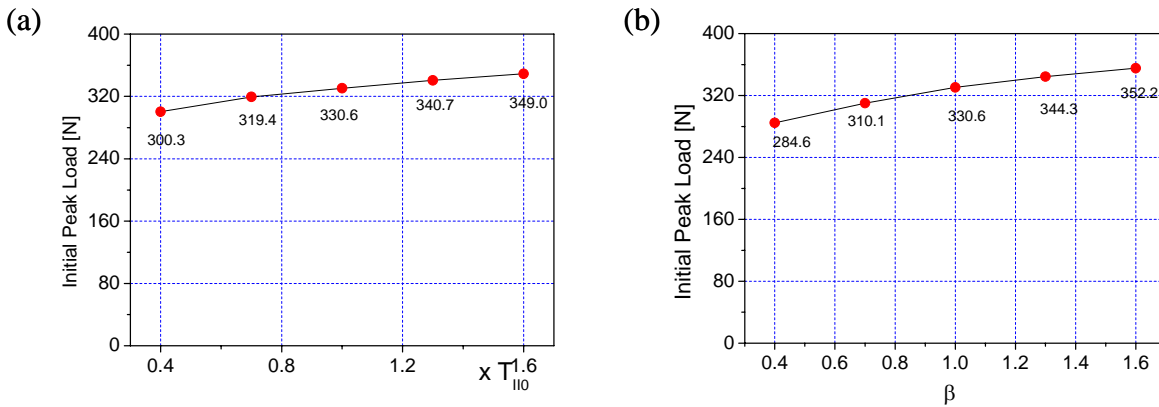


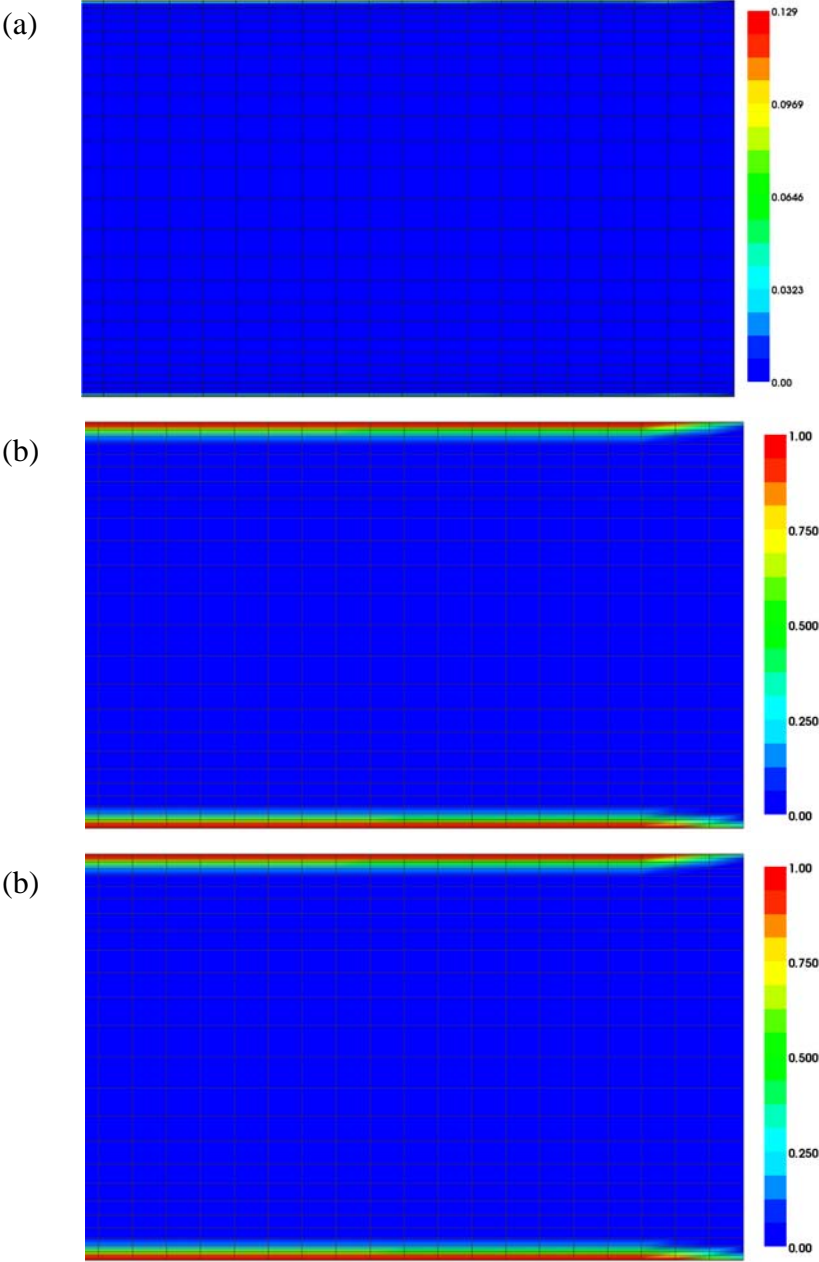
Figure 8. Initial peak load of ENF specimens; (a) peak load vs. τ_1^0 and (b) peak load vs. β

Mixed-mode fracture

The composite laminate with a stacking sequence of $[+30/-30/90/NL/90/-30/+30]_T$ is subjected to uniaxial tension loading. The test specimen has a length, width and thickness of 254 mm, 25.4 mm and 8.382 mm, respectively.

For the FE analysis, the specimen was discretized with $120 \times 30 \times 6$ 8-node hexahedral elements (90024 DOFs), and the interface elements with the exponential CZM ($\beta = 1.5$) were placed in the middle of the $[90/90]$ interlayer to simulate the initiation and propagation of the delamination. Since the damage is mainly caused by the stress concentration in the free-edge region, the specimen was modeled in such a way that the FE mesh was refined from the center toward the free edges. The displacement-controlled Newton-Raphson technique with automatic increment adjustment and the line search algorithm were employed to obtain the converged solution of the nonlinear equations.

Figure 13 shows the evolution of delamination damage represented by the contour of damage variable with the strain increase. The value of damage variables greater than zero and equal to one imply the initiation and propagation of the delamination, respectively.



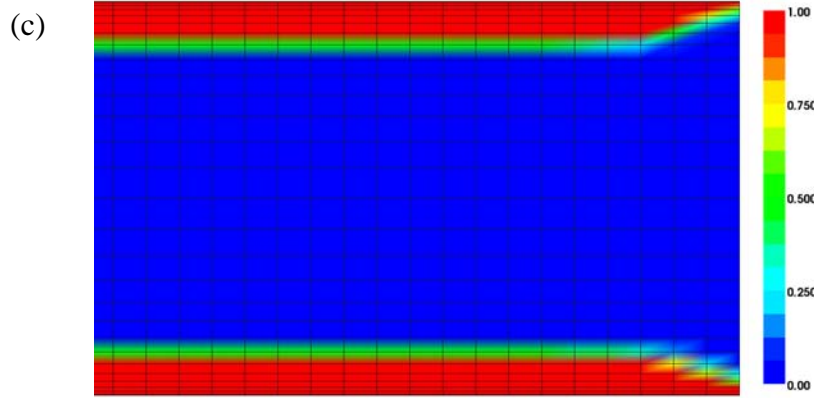


Figure 9. Contours of damage at various strain levels of (a) $\varepsilon = 0.55\%$, (b) $\varepsilon = 0.69\%$ and (c) $\varepsilon = 1.18\%$.

The load and strain values at which delamination initiates (T_c and ε_c) and complete detachment (T_p and ε_p) occurs for different critical energy release rates are summarized in Table 2.

Table 2. Load/strain of delamination initiation/propagation

G_{IC} (N/m)	G_{IIC} (N/m)	T_c (N)	ε_c (%)	T_p (N)	ε_p (%)
184	490	6200	0.43	8640	0.65
263	701	7042	0.49	9800	0.70
328	911	7900	0.55	11700	0.83

3 EXPERIMENT

Experiment was performed with the laminated composites reinforced with nano-interlayers to evaluate the microcrack- and delamination-resistance performance. We considered the cases with the nano-interlayers made in the form of (a) thin film of epoxy material reinforced with the VGCNFs and (b) fiber mat that was fabricated with the electrospun process.

3.1 Film nano-interlayer

The baseline layup is $[+30/-30/90]_s$, where the subscript s represents a symmetric layup. With the baseline layup, one, three and five nano-interlayers can be placed between the composite layers to make $[+30/-30/90/NL]_s$, $[+30/-30/NL/90/NL]_s$, $[+30/NL/-30/NL/90/NL]_s$, respectively, where NL represents the nano-interlayer. The nano-interlayer was fabricated in the form of thin film with epoxy material reinforced with VGCNFs.

The laminated composites of the $[+30/-30/90]_s$ layup were loaded under uniaxial tension loading at a stress level of 50 ksi. The free edge of the test specimen was polished and observed with a microscope. Figure 10 shows the micrographs taken at the free edge of the specimen with and

without the nano-interlayer. As the analysis predicts, severe interlaminar stress causes delamination in the middle of the test specimen between the [90/90] layup, which thus causes extensive delamination, as shown in a micrograph in Figure 10 (a). With the presence of the nano-interlayer, the interlaminar stress concentration is relieved to help the reduction of the severity of delamination damage as shown in Figure 10 (b).

Figure 11 (a) shows the numbers of microcracks in a 6-inch span at various stress levels under uniaxial tension loading. The hollow rectangle and solid circular markers represent the crack counts without and with the nano-interlayers, respectively. The figure clearly shows that existence of the nano-interlayer in the laminated composites suppresses the microcracks with the increase of the loading. Figure 11 (b) shows the stress level at the initiation of the delamination without and with the nano-interlayers. We can observe a significant increase of the delamination initiation stress with the presence of the nano-interlayer.

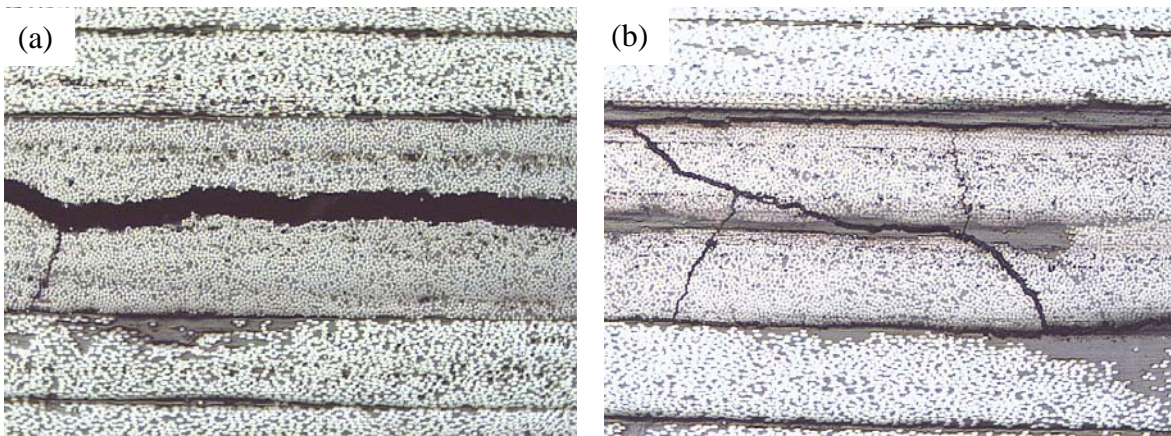


Figure 10. Micrographs with microcracks and delamination under a uniaxial tension loading at a stress level of 50 ksi: (a) no nano-interlayer $[+30/-30/90]_s$ and (b) with nano-interlayer $[+30/-30/NL/90/NL]_s$.

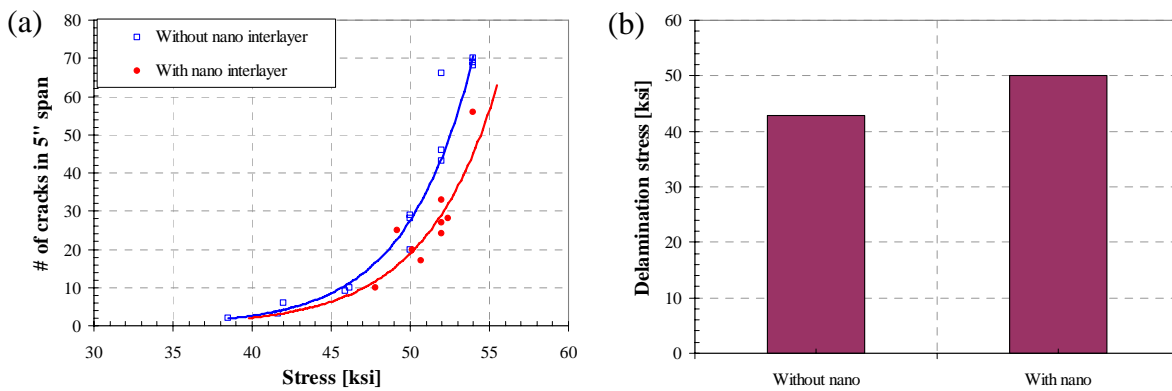


Figure 11 (a) Number of microcracks counted in a 6-inch span in the middle of the test specimen at various stress levels and (b) delamination stress with and without the nano-interlayers under uniaxial tension loading.

3.2 Electrospun nano-interlayer

The present work considers the electrospun fiber mat as the nano-interlayer to relieve the interlaminar stress concentration. The fiber mats were fabricated with the in-house electrospun machine built at Soongsil University in Korea. The fiber mats were delivered to the University of Dayton Research Institute (UDRI) to be ready to put between the composite layers. Once fabricated and processed, the test specimens with layups of $[+30/(NL)/-30/(NL)/90/(NL)]_s$ were prepared for similar uniaxial tension tests that were explained earlier in a previous section, where (NL) indicates a possible location of the insertion of the nano-interlayer. Therefore, five nano-interlayers were inserted between the laminate plies. As shown in the numerical calculation, these nano-interlayers are expected to suppress/delay the delamination damage by reducing the interlaminar stress concentration at the free edge.

The test specimens were loaded under uniaxial tension with the MTS machine. An acoustic emission device was used to monitor the damage events due to the microcracks and delamination during the loading. Once the events were observed, we stopped the load increase and monitored the microcracking and delamination damage by using an optical microscope. At this time, we counted the number of microcracks and delamination and took some micrographs. The micrographs were taken for the test specimens before loading (Figure 12), at the first-ply failure (Figure 13) and after the first observation of delamination (Figure 14). In these figures, the micrographs on the left-hand-side and right-hand side represent the specimens without and with the nano-interlayers, respectively. Figure 12 clearly shows the existence of the nano-interlayers. The thicknesses measured from five specimens without the nano-interlayers and five specimens with the five nano-interlayers are approximately 1.229 mm (0.0484 in) and 1.229 mm (0.0484 in), respectively. Therefore, the total thickness of the five nano-interlayers from the electrospun mat is less than 0.001 mm, which is significantly thinner than the other existing interleave layers.

Figure 13 shows the single vertical microcrack that is observed at the free edge of the specimens without and with the nano-interlayers after they were loaded to 165.2 MPa (24.0 ksi) and 171.2 MPa (24.8 ksi), respectively. The averages of the FPF stress with the five pristine and five nano specimens are 175.3 MPa (25.4 ksi) and 184.4 MPa (26.8 ksi), respectively. Therefore, we observed a 5.2% increase of the FPF stress with the addition of the nano-interlayers. Figure 14 shows both the vertical microcrack and the horizontal delamination that are observed at the free edge of the specimens without and with the nano-interlayers after they were loaded to 246.0 MPa (35.8 ksi) and 271.1 MPa (39.3 ksi), respectively. The averages of the delamination stress with the five pristine and five nano specimens are 249.1 MPa (36.1 ksi) and 269.1 MPa (39.0 ksi), respectively. Therefore, we observed an 8.0% increase of the delamination stress with the addition of the nano-interlayers. The averages of the numbers of microcracks at the delamination stress with the five pristine and five nano specimens are 64 and 50, respectively, which is a 21.6% decrease with the addition of the nano-interlayers. Therefore, we can conclude that the nano-interlayer can suppress the microcracking and delamination damage. The averages

of the ultimate strength with the five pristine and five nano specimens are 296.0 MPa (42.9 ksi) and 324.9 MPa (47.1 ksi), respectively. Therefore, we observed a 9.8% increase of the ultimate strength with the addition of the nano-interlayer.

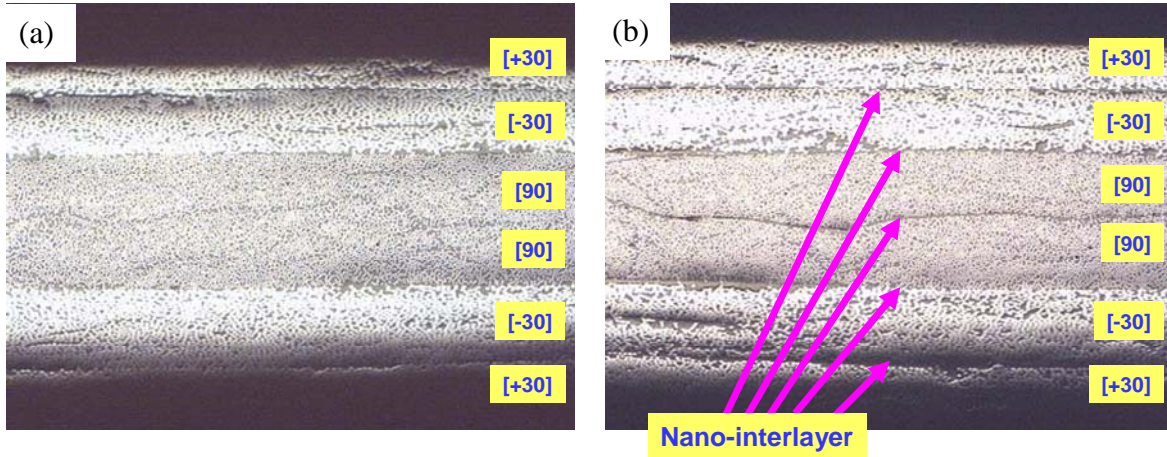


Figure 12. Micrographs of test specimens before loading: (a) without nano-interlayer $[+30/-30/90]_s$ and (b) with nano-interlayer $[+30/NL/-30/NL/90/NL]_s$.

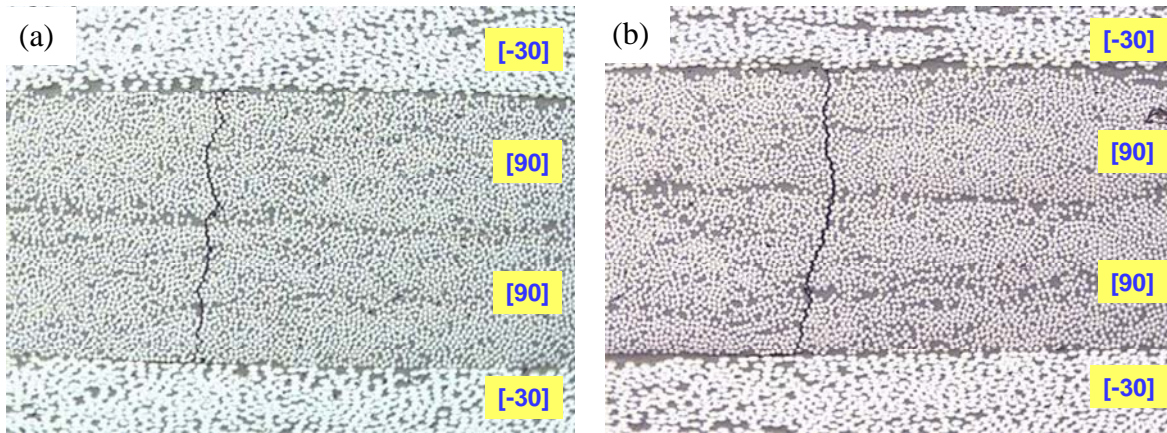


Figure 13. Micrographs with a microcrack at the first-ply failure under a uniaxial tension loading at a stress level of (a) 165.2 MPa (24.0 ksi) without nano-interlayer $[+30/-30/90]_s$ and (b) 171.2 MPa (24.8 ksi) with nano-interlayer $[+30/-30/NL/90/NL]_s$.

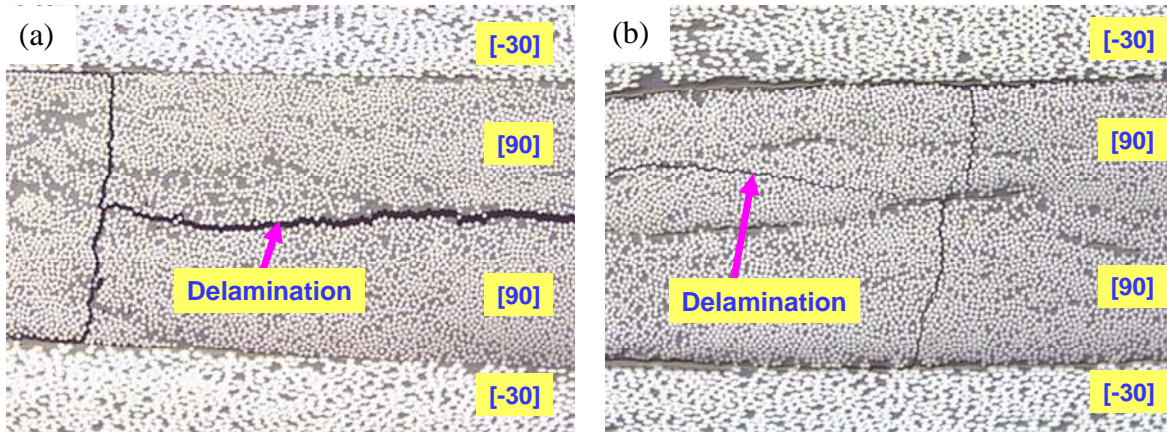


Figure 14. Micrographs after the first observation of delamination under a uniaxial tension loading at a stress level of (a) 246.0 MPa (35.8 ksi) without nano-interlayer $[+30/-30/90]_s$ and (b) 261.5 MPa (37.9 ksi) with nano-interlayer $[+30/-30/NL/90/NL]_s$.

Figure 15(a) shows the number of the microcracks counted in a 6-inch span at the free edge in the middle of the test specimen at various stress levels. The hollow dots with a dotted line and solid dots with a solid line represent the data from the five specimens without and with the nano-interlayer, respectively. The figure clearly shows that the number of microcracks is decreased with the addition of the nano-interlayers at several stress levels.

Figure 15(b) shows stress levels at the first-ply failure, delamination and ultimate failure with and without the nano-interlayers under uniaxial tension loading. As stated above, the stress levels at the first-ply failure, delamination and ultimate failure increased 5.2%, 8.0% and 9.8% with the addition of the nano-interlayers, respectively. Therefore, we can conclude that the presence of the nano-interlayer can decrease and/or suppress the microcracking and delamination damage by reducing the interlaminar stress concentration at the free edges in the laminated composites.

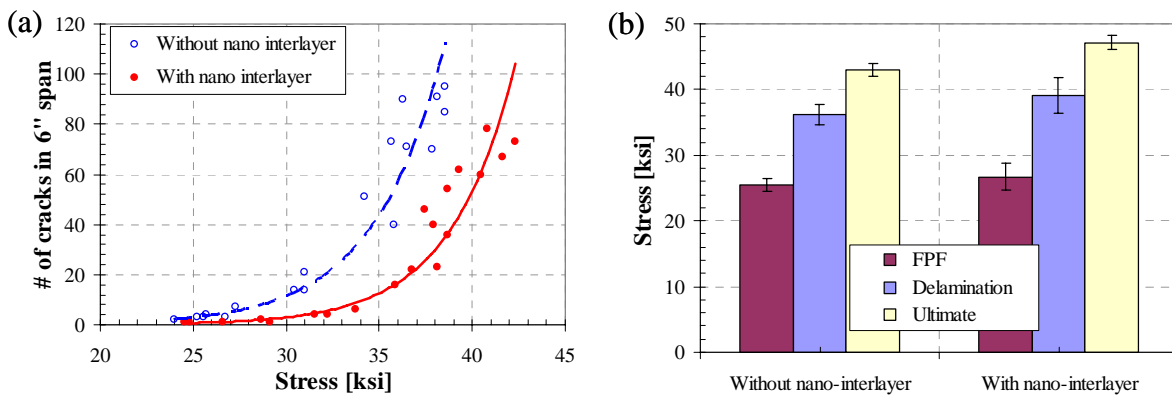


Figure 15. (a) Number of microcracks counted in a 6-inch span at the free edge in the middle of the test specimen at various stress levels and (b) stress levels at the first-ply failure,

delamination and ultimate failure with and without the nano-interlayers under uniaxial tension loading.

4 CONCLUSIONS

Computational and experimental studies were carried out for the laminated composites reinforced with nano-interlayers that were fabricated in the form of either a thin film of nano-modified epoxy reinforced with VGCNFs or a fiber mat that can be fabricated with the electrospun fiber process. The computation model used a CZM with interface elements based on bilinear and exponential constitutive laws. The model was used to simulate mode I, mode II and mixed-mode fracture tests to assess initiation and progression of delamination characteristics of the laminated composites.

From a numerical parametric study for the mode I fracture with a DCB test, we found that the maximum load is mostly dependent on the critical energy release rate (G_{IC}) with the bilinear constitutive law. Interfacial strength and penalty parameter play fewer roles in determining the maximum load. Parametric studies were carried out for mode II, an ENF test, to assess the delamination characteristics corresponding to different parameters of the exponential constitutive law. Finally, uniaxial tension simulations were carried out for the [-30/30/90/NL]_s specimen to predict the free-edge delamination characteristics corresponding to different interface properties.

Experimental observation from micrographs and stress-strain behavior shows that the laminated composites with nano-interlayers can suppress the stress concentration and severity of the microcrack and delamination damage. In addition to the potential enhancement of the multifunctionality due to its superior material properties, such as thermal and/or electrical conductivity, less thermal mismatch, etc., the improvement of the mechanical performance with the nano-interlayer draws further investigation of the nano-interlayer study.

ACKNOWLEDGEMENTS

The authors would like to thank Ron Esterline of the University of Dayton Research Institute for sample preparation and testing. This work was performed under U.S. Air Force Contract No. FA8650-05-D-5052.

5 REFERENCES

1. P. P. Camanho, C. G. Dávila and M. F. de Moura, J. of Composite Materials, **37**, 1415-1438 (2003).
2. V. K. Goyal, E. R. Johnson, C. G. and Dávila, Proc. of 43rd AIAA/ASME/ASCE/AHS/ASC Structures, Structural Dynamics, and Materials Conference, AIAA 2002-1576, 12 (2002).
3. J. H. Kim, C. S. Lee and S. J. Kim, AIAA Journal, **43**, 662-670 (2005).